Supplement of Eur. J. Mineral., 36, 943–983, 2024
https://doi.org/10.5194/ejm-36-943-2024-supplement

European Journal of Mineralogy
Open Access

Supplement of

Pressure–temperature–time and REE mineral evolution in low- to medium-grade polymetamorphic units (Austroalpine Unit, Eastern Alps)

Marianne Sophie Hollinetz et al.

Correspondence to: Marianne Sophie Hollinetz (marianne.sophie.hollinetz@univie.ac.at)

S1. Methods used for rock and mineral characterization

The sample preparation and general petrographic characterization was carried out at the University of Vienna (Austria). Polished thick sections were investigated using a FEI inspect S scanning electron microscope (SEM) equipped with a tungsten hairpin electron source and an EDAX Pegasus Apex 4 system consisting of an Apollo XV Silicon Drift Detector. For image acquisition, the instrument was operated in back-scattered electron (BSE) mode at 15 kV acceleration voltage, 10 mm working distance and a spot size varying between 3-6 (dimensionless, refers to a certain configuration of the lenses).

Quantitative mineral chemistry analyses were determined using a field emission gun Cameca SXFiveFE electron probe microanalyzer (EPMA) equipped with a Schottky field emission gun electron source and five wavelength-dispersive spectrometers (WDS). Operating conditions were 15 kV acceleration voltage and a beam current of 20 nA for garnet, staurolite, chloritoid, ilmenite and plagioclase. Phyllosilicates were measured with a beam current of 10 nA and a defocused beam diameter of 5 µm to minimize beam damage. Plagioclase was measured with a defocused beam diameter of 7 µm and 10 s peak counting time to avoid Na-loss. Counting times for other elements are 20 and 10 s at peak position and background, respectively. Natural and synthetic minerals were used as standards (Ntaflos et al., 2017). Major element compositions of biotite, chlorite, chloritoid, garnet, ilmenite, plagioclase, staurolite and white mica and calculated mineral formulae are reported in Tables S1-S8. Major and trace element compositions of allanite, monazite, xenotime and thorite were analyzed using 20 kV acceleration voltage and 100 nA beam current. For allanite, the beam was defocused to 3-5 µm. La, Ce, Nd, Eu, Dy, and Y were measured using the Lα line and 25 s peak counting time. Pr, Sm, Gd and Er were measured using the Lβ line and 30 s peak counting time. For Th and U, the Mα and Mβ lines and 35.5 s and 30 s peak counting time were used, respectively. For Pb, the Lα line was measured for 40 s at peak position at two spectrometers simultaneously. For fluorapatite analyses 20 kV acceleration voltage, 20 nA beam current and a defocused beam diameter of 8 µm was used. Na, F and Cl were measured first with 10 s peak counting time. Synthetic glasses were used for calibration. Results of REE-minerals are in Tables S9–S11. The PAP method (Pouchou and Pichoir, 1991) was used for matrix correction for all data. The laboratory internal standard yields a relative error below 1% (Ntaflos et al., 2017).

Semiquantitative element maps of allanite /REE-epidote of sample Ra-4 were acquired using the Cameca SXFiveFE EMPA (University of Vienna, Austria) using the Lα line for La, Nd and Y and the Mα line for Th. Maps were produced at 20 kV acceleration voltage and 100 nA beam current using a step size of 1-1.5 µm and dwell time of 0.04 s. Additional semiquantitative element maps of allanite in sample Hi-1 and

monazite in sample Ro-2 were acquired using a Vega-II Tescan SEM at the Geological Survey of Austria, Vienna, which is equipped with an X-Max 50 mm^2 Oxford Instrument EDS detector operated by AZTec software. Maps were collected using the following settings: 15 kV acceleration voltage, 70 nA beam current, 27 mm working distance, 0–10 keV range, 1024 bins (corresponding to ~0.3 µm stepsize). The raw count data of all element maps was processed using a smoothing filter for noise reduction (Savitzky and Golay, 1964). To enhance concentration gradients, the data was normalized and plotted with a gamma correction using exponent values between 0.6 and 2 (Heilbronner and Barrett, 2013).

Samples selected for whole rock analyses were cleaned from macroscopic signs of alteration, crushed and ground to a fine powder using an agate disc mill. Major and trace elements were determined by inductively coupled plasma mass spectrometry (ICP-MS) of fused beads at Activation Laboratories Ltd. (Ancaster, Canada) using the 4 Litho package. Analyses of internal duplicates yield analytical uncertainties of <2.6% for major elements (except MnO, 3.4%) and <7.6% for REEs, Th and U.

S2. Laser ablation inductively coupled plasma mass spectrometry (LA-ICP-MS)

The U-Th-Pb analyses were performed using a Resonetics M-50 193 nm ArF Excimer laser ablation system coupled to an Agilent 7700x quadrupole ICP-MS system at the University of New Brunswick (UNB), Canada, following the protocol of McFarlane and Luo (2012). Samples and standards were loaded in a Laurin Technic Pty S-155 two-volume cell with a working ablation volume of < 1 cm^3. Reference material NIST610 with isotope values for Pb/U from Horn and von Blanckenburg (2007) was used as primary standard. Prior to each analytical session, tuning of the ICP-MS on NIST610 glass to achieve $^{248}ThO/^{232}Th < 0.2\%$, $^{238}U/^{232}Th \sim 1.05$, and $^{44}Ca^{++}/^{44}Ca^{+} \leq 0.2\%$ was carried out to maximize sensitivity and minimize interference-related biases in final corrected ages.

Target grains were localized based on SEM documentation in combination with micro X-ray fluorescence compositional maps produced by a Bruker M4 Tornado (UNB). Allanite / REE-epidote was analyzed using a 24 µm crater diameter, 1.2 to 1.5 J/cm^2 laser fluence, 3 Hz repetition rate and 25 s of sample ablation preceded by 30 s background collection. Allanite was standardized against NIST610 according to the protocol of McFarlane (2016). To monitor reproducibility, Siss3 allanite (c. 33 Ma, Oberli et al., 2004) and Hartfield intrusion allanite (c. 414 Ma, McFarlane, 2016) were used as reference material. Monazite was ablated using a 10 µm crater diameter, 3 J/cm^2 laser fluence, 4 Hz repetition rate and 30 s background measurement preceding 30 s sample ablation. GSC8153 monazite (c. 507 Ma) was used as a primary standard and 44069-monazite (c. 425 Ma, Aleinikoff et al., 2006) was used as a secondary

standard. The ablated material was transferred in a carrier gas composed of 930 mL/min Ar and 300 mL/min He via a Laurin Technic Pty Peek^{TM} Y-connector and 'squid' smoothing device to the ICP-MS. The following masses were analyzed with dwell times in ms given in brackets: ^{202}Hg (20), ^{204}Pb, Hg (60), ^{206}Pb (50), ^{207}Pb (70), ^{208}Pb (10), ^{232}Th (10) and ^{238}U (20). Additionally, the following masses were monitored using a dwell time of 10 ms: ^{31}P, ^{44}Ca ^{49}Ti, ^{56}Fe, ^{90}Zr, ^{89}Y, ^{139}La and ^{146}Nd. Concentrations of these elements are calculated without internal standard but are typically within 20% of the true value, thus sufficient for the purpose of detecting inclusions and assigning individual U-Pb analyses to chemical domains of the analyzed unknowns.

Data reduction was carried out offline using Iolite v3.7 (Paton et al., 2011) in combination with VizualAge v2015.06 (Petrus and Kamber, 2012) running under Wavemetrics IgorPro v6.22. The U-Pb geochronology data reduction scheme of Iolite (Paton et al., 2010) performs a down-hole Pb/U fractionation correction, followed by a drift correction, reference material normalization and uncertainty propagation. Analyses exhibiting obvious heterogeneity in the time-resolved U-Pb concentrations were removed during this step. Common Pb corrected values for monazite of sample Ro-2 based on measured net ^{204}Pb were calculated using Isoplot 3.71 (Ludwig, 2012). Tera-Wasserburg Concordia diagrams, joint isochron regression ages and mean weighted mean age plots are produced using IsoplotR 6.0 (Vermeesch, 2018).

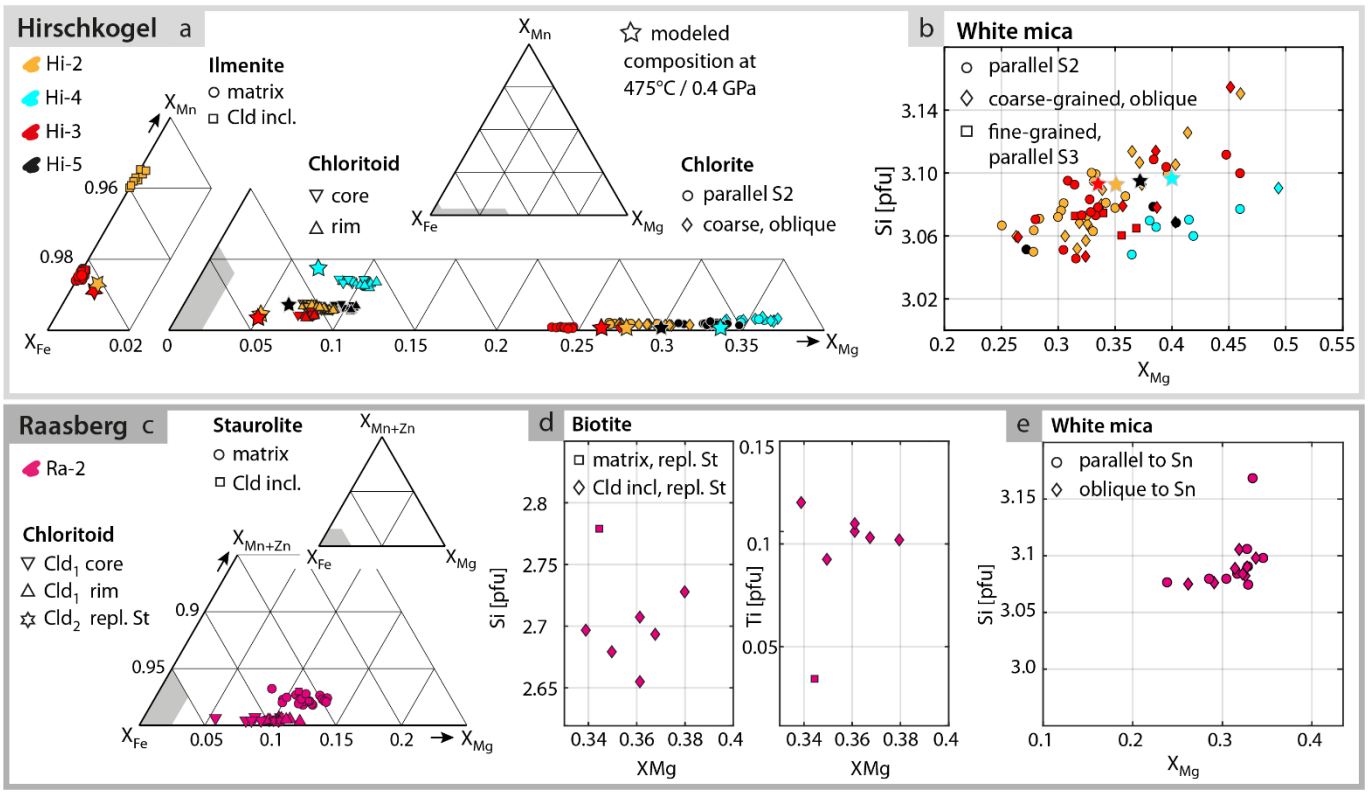

Figure S1. EPMA data of main minerals for additional Hirschkogel (a-b) and Raasberg (c-e) samples. (a) XFe – XMg – XMn ternary plot of chloritoid, chlorite and ilmenite. (b) XMg – Si pfu binary plot of white mica. (c) XFe – XMg – XMn ternary plot of staurolite and chloritoid, (d)) XMg – Si pfu and XMg – Ti pfu binary plots of biotite and (d) XMg – Si pfu plot of white mica in sample Ra-2.

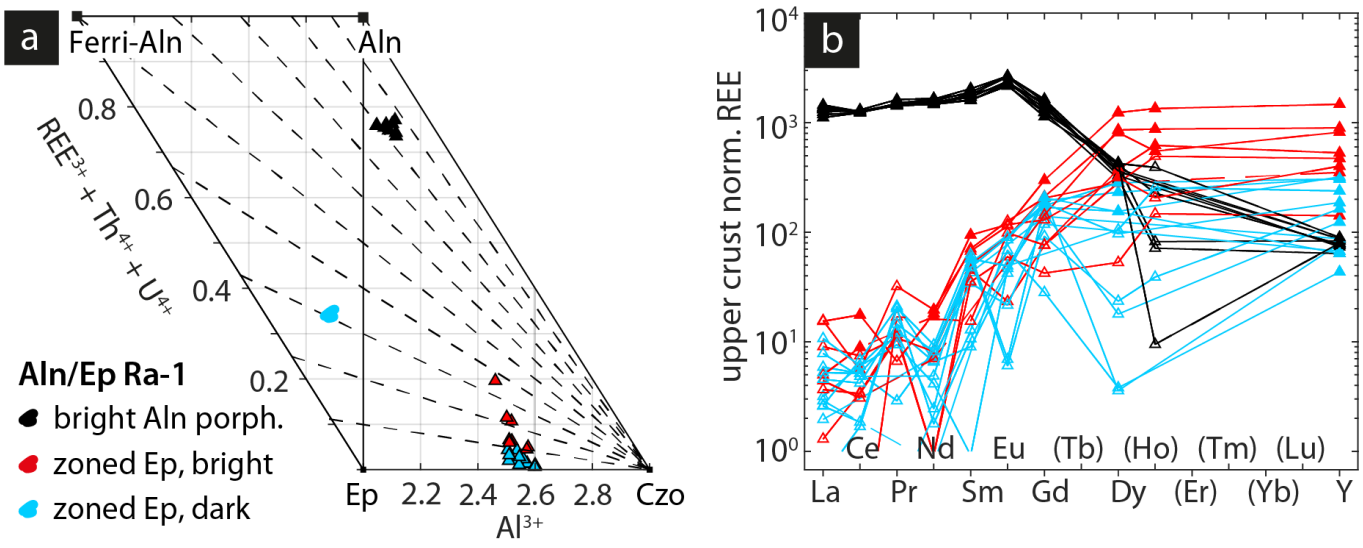

Figure S2. Additional EPMA data of allanite and REE-epidote in sample Ra-1. (**a**) Al – REE+U+Th diagram illustrating compositional variation in the clinozoiste – epidote – ferriallanite – allanite system and (**b**) REE distribution of allanite and REE-epidote relative to the average upper crust (Rudnick and Gao, 2003).

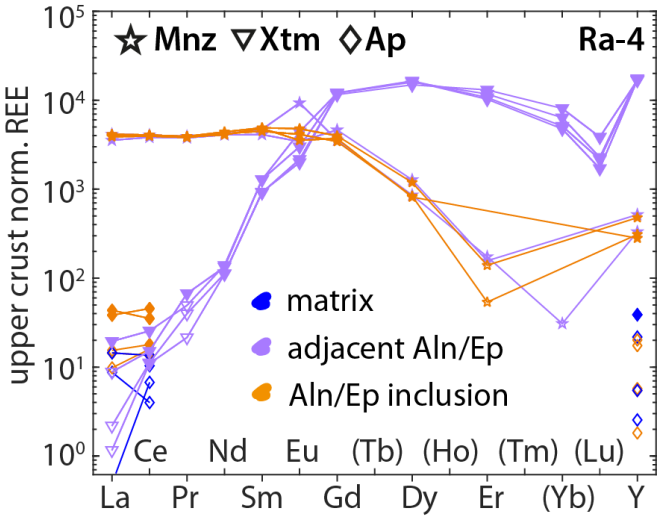

Figure S3. REE distribution of monazite, xenotime, thorite and apatite of sample Ra-4 normalized relative to the average upper crust (Rudnick and Gao, 2003).

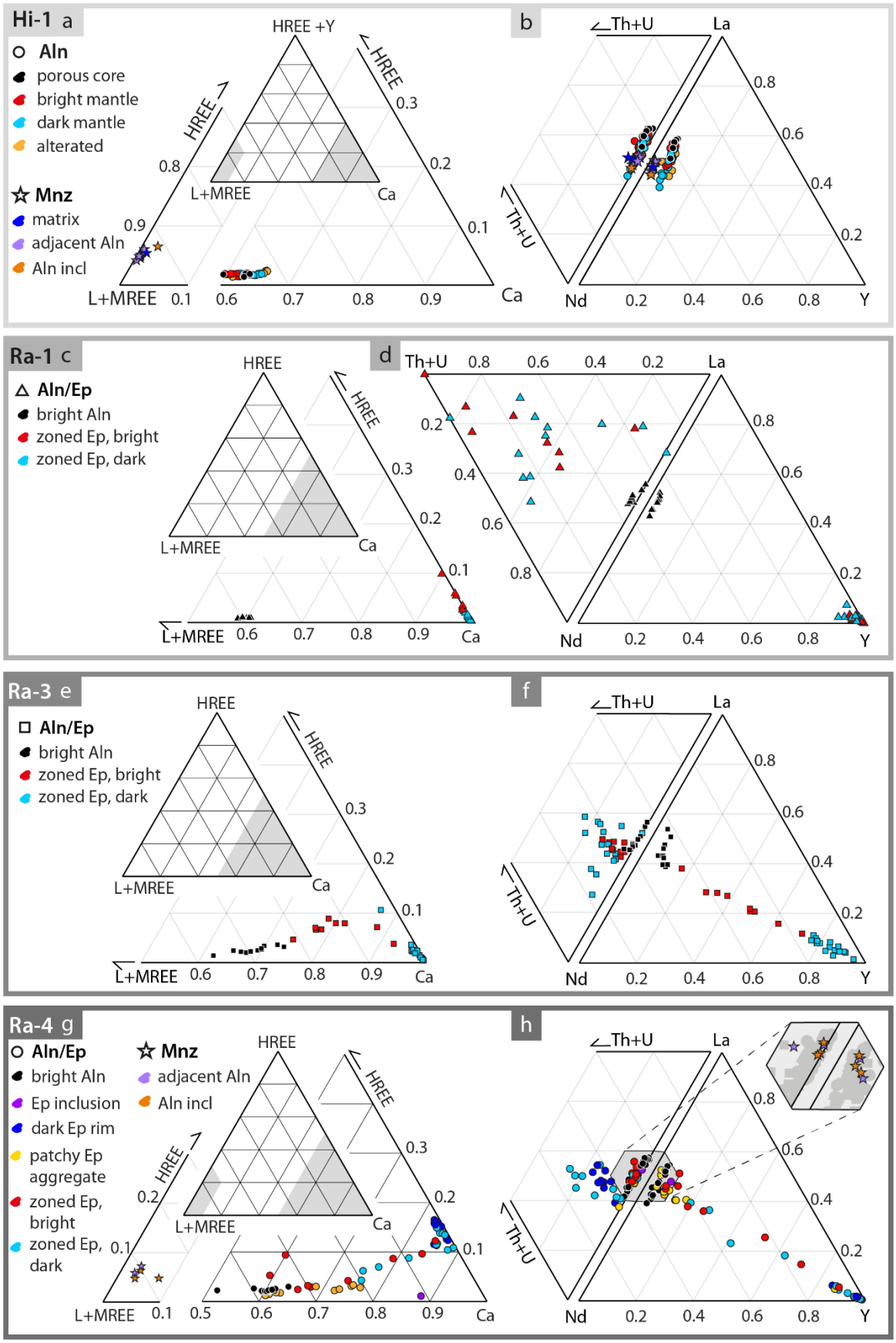
Hi-1 a
Aln
porous core
bright mantle
dark mantle
altered
Mnz
matrix
adjacent Aln
Aln incl
HREE +Y
HREE
L+MREE
Ca
b
Th+U
La
Nd
Y
Ra-1 c
Aln/Ep
bright Aln
zoned Ep, bright
zoned Ep, dark
d
Ra-3 e
f
Ra-4 g
Aln/Ep
bright Aln
Ep inclusion
dark Ep rim
patchy Ep aggregate
zoned Ep, bright
zoned Ep, dark
Mnz
adjacent Aln
Aln incl
h

Figure S4. (**a, c, e, g**) L+MREE-Ca-HREE ternary plots and (**b, d, f, h**) La-Nd-Th+U and La-Nd-Y ternary plots of allanite, REE-epidote and monazite in samples Hi-1, Ra-1, Ra-3 and Ra-4. Note that a different color code applies for each sample.

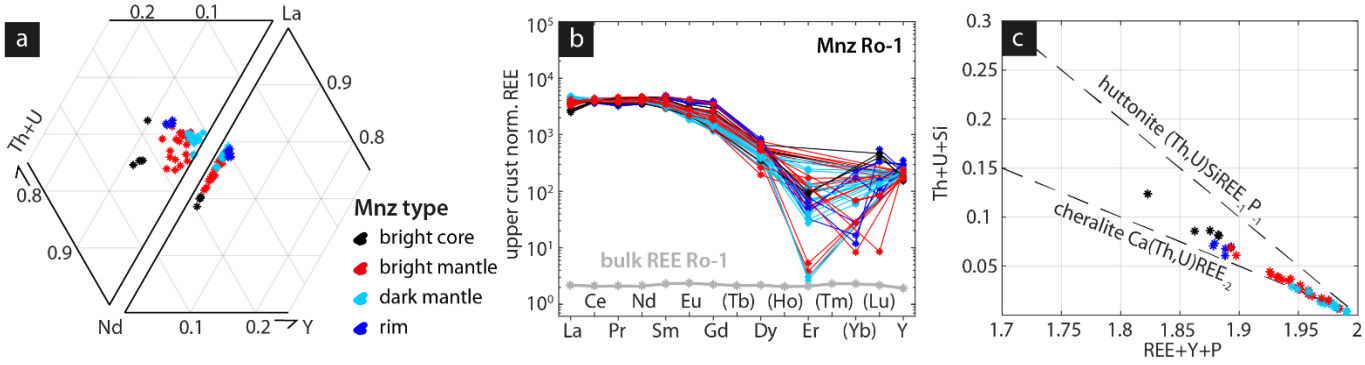

Figure S5. (**a**) La-Nd-Th+U and La-Nd-Y ternary plots, (**b**) REE distribution normalized by the average upper crust of Rudnick and Gao (2003), and (**c**) REE+P vs. Th+U+Si (pfu) showing huttonite and cheralite substitutions of monazite in sample Ro-1. Elements in brackets were not analyzed in all datasets.

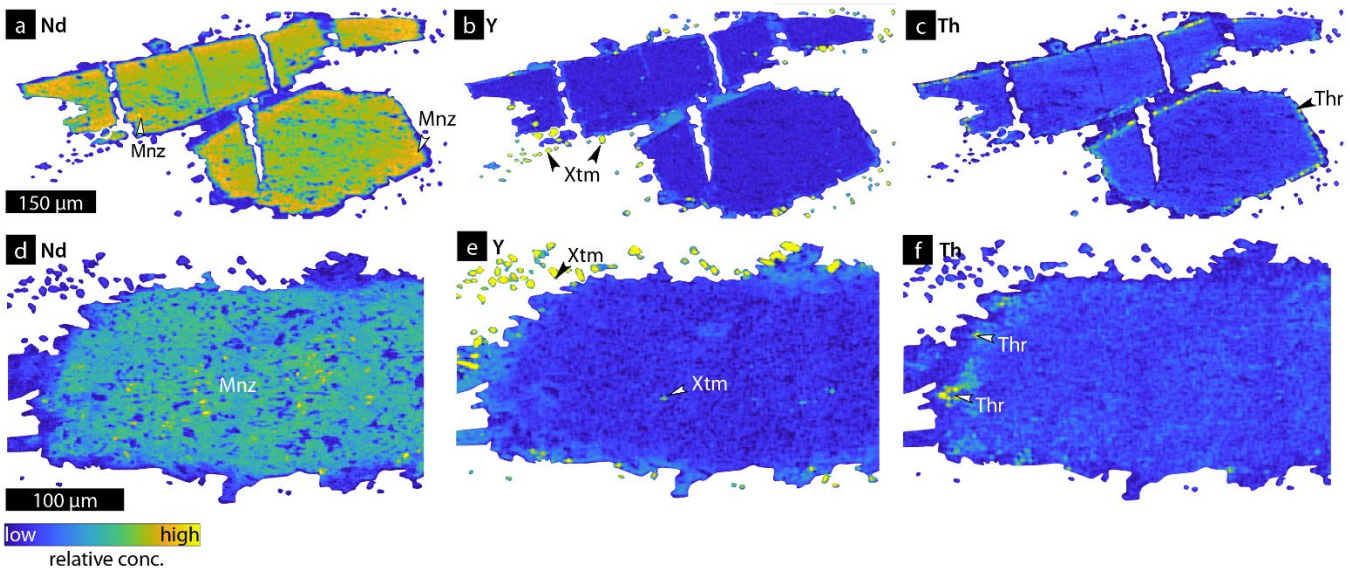

Figure S6. Compositional maps of allanite and REE-epidote of sample Ra-4. (**a**) Nd, (**b**) Y and (**c**) Th distribution of allanite / REE-epidote shown on Fig. 9e. (**d**) Nd, (**e**) Y and (**f**) Th distribution of patchy REE-epidote shown on Fig. 9h.

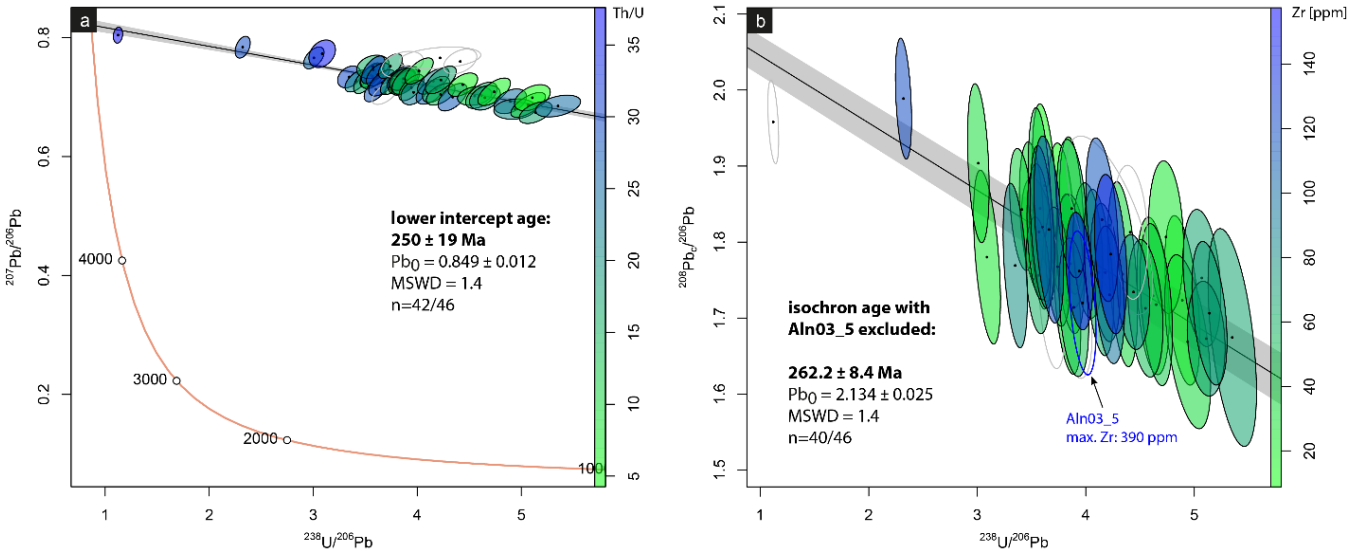

Figure S7. Additional plots of LA-ICP-MS U-Th-Pb analyses of allanite in sample Hi-1. (a) Tera-Wasserburg diagram and lower intercept date. (b) Total Pb/U-Th isochron color-coded by Zr, indicating that tiny zircon inclusion do not bias the age.

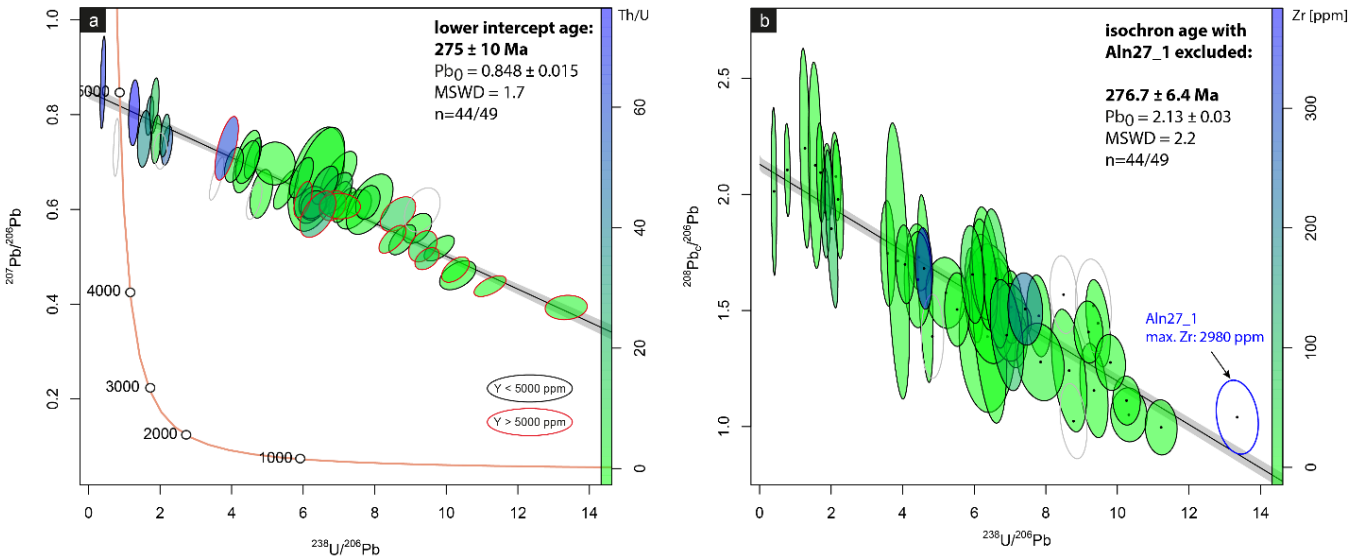

Figure S8. Additional plots of LA-ICP-MS U-Th-Pb analyses of allanite in sample Ra-3. (a) Tera-Wasserburg diagram and lower intercept date. (b) Total Pb/U-Th isochron color-coded by Zr. The isochron date excluding analysis Aln27_1with elevated Zr content yields an age that is identical within error.

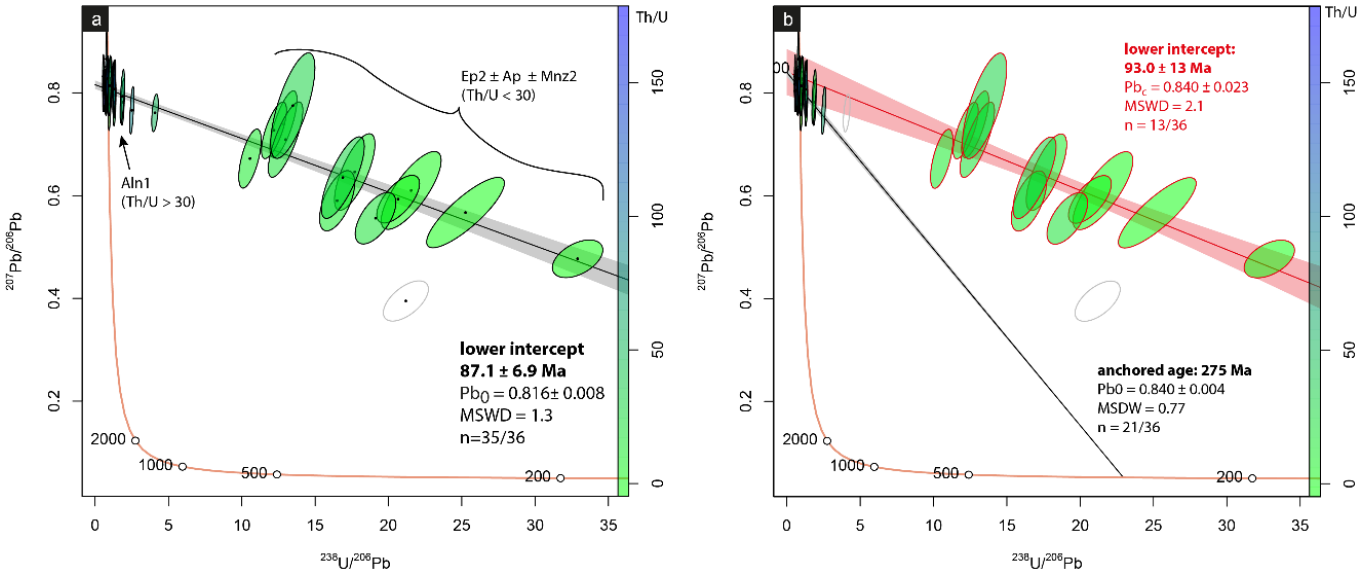

Figure S9. Additional plots of LA-ICP-MS U-Th-Pb analyses of allanite in sample Ra-4. (a) Tera-Wasserburg diagram and lower intercept date calculated from both high and low Th/U population, corresponding to Aln_1 and Ep_2 generations. (b) Tera-Wasserburg diagram with separate regressions calculated for low Th/U population (red) and high Th/U population.

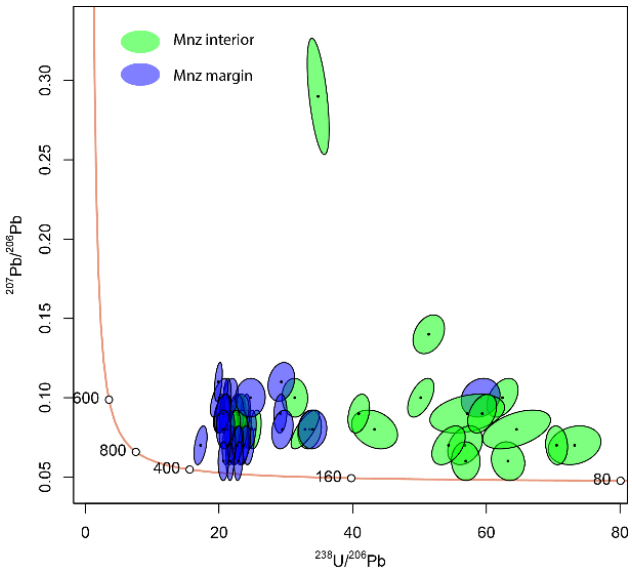

Figure S10. Tera-Wasserburg diagram of uncorrected U-Pb data of monazite in sample Ro-2.

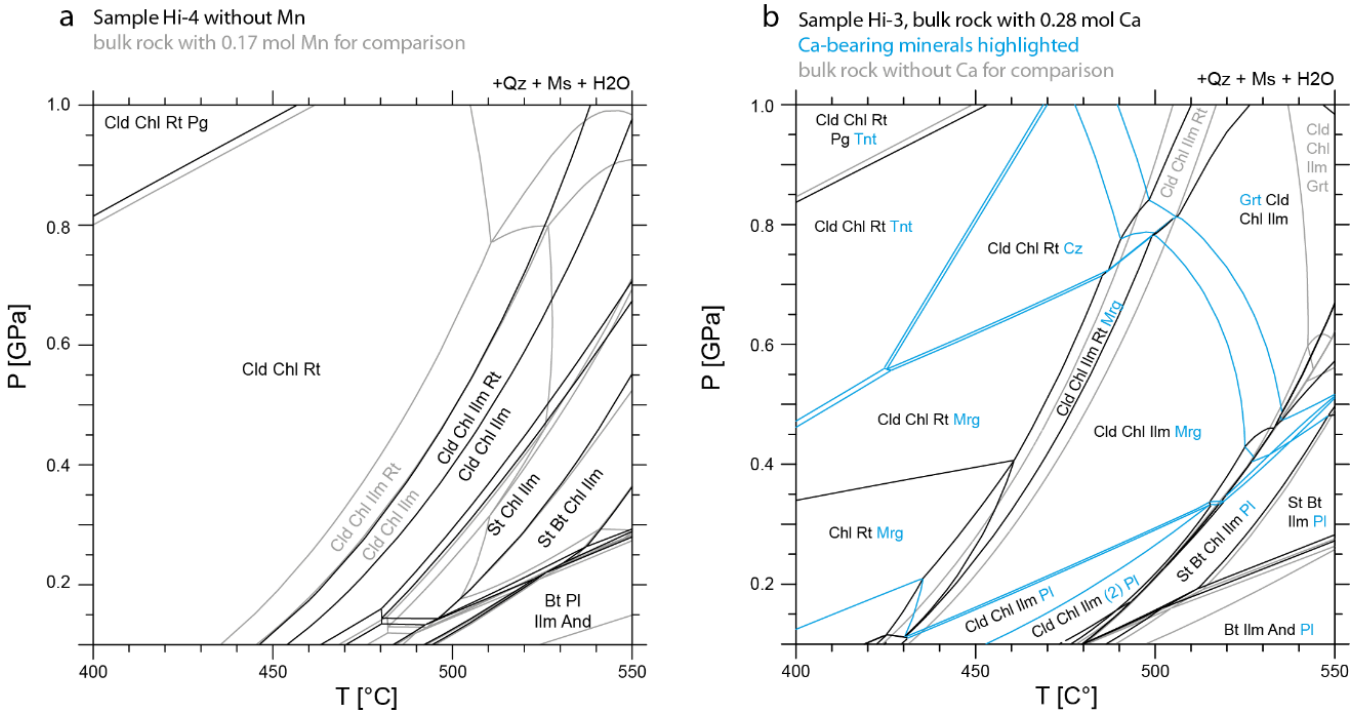

Figure S11. Pseudosections for selected Hirschkogel samples testing effects of bulk composition variations. (**a**) Pseudosection of sample Hi-4 without Mn. (**b**) Pseudosection of sample Hi-3 calculated with uncorrected Ca composition. Ca-bearing phases are highlighted in blue.

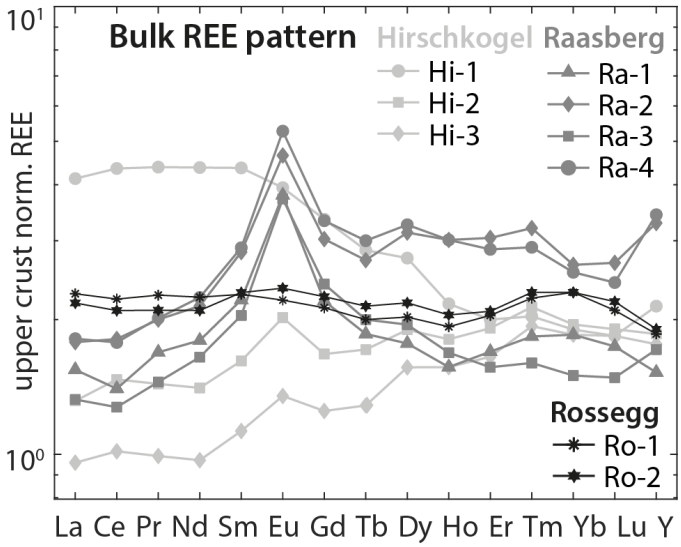

Figure S12. Bulk rock REE compositions normalized by the average upper crust (Rudnick and Gao, 2003).

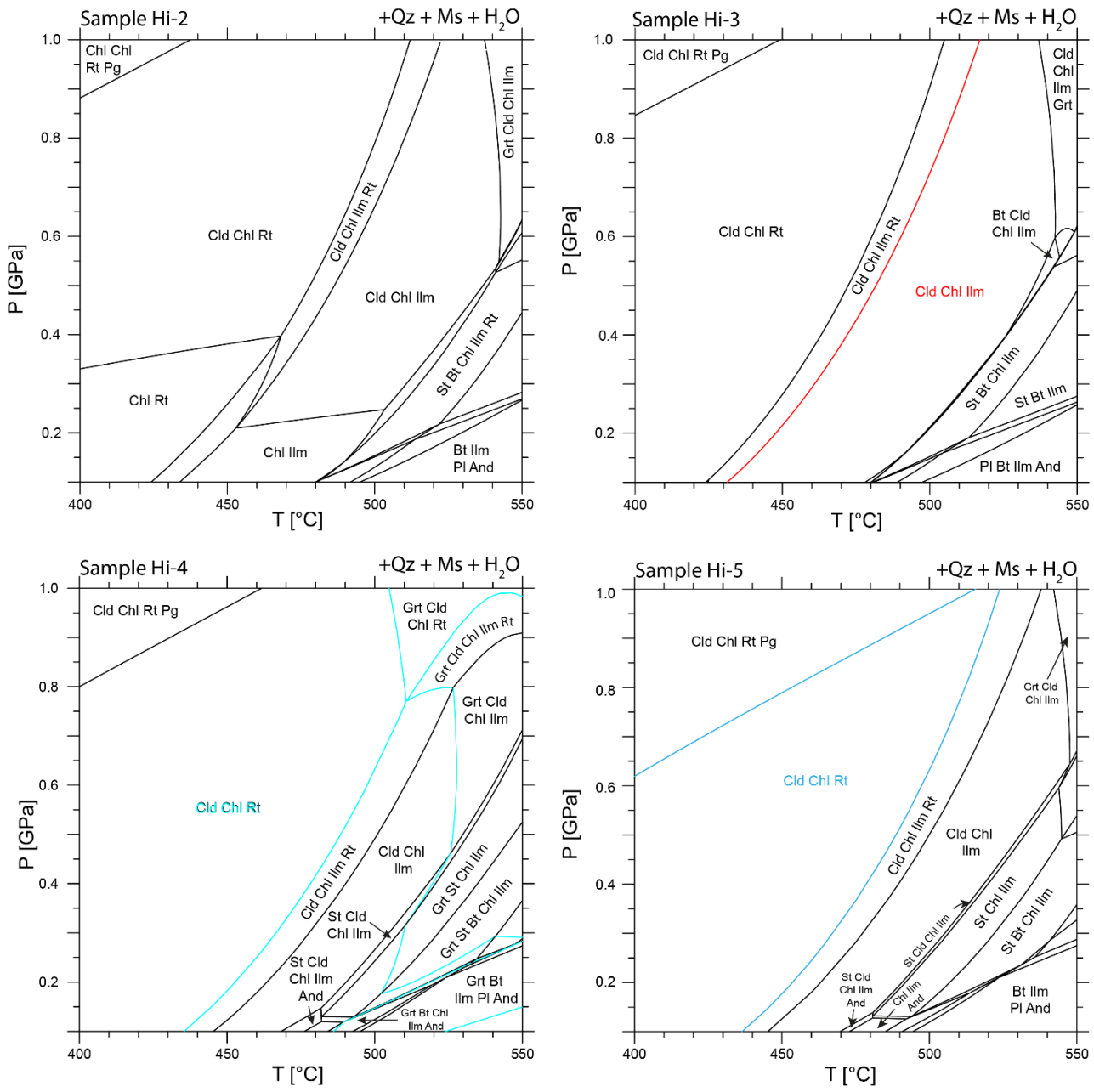

Figure S13. Pseudosections of additional Hirschkogel samples. Reactions shown in Fig. 3f and the Permian peak assemblage are highlighted.

References

Aleinikoff, J. N., Schenck, W. S., Plank, M. O., Srogi, L., Fanning, C. M., Kamo, S. L., and Bosbyshell, H.: Deciphering igneous and metamorphic events in high-grade rocks of the Wilmington Complex, Delaware: Morphology, cathodoluminescence and backscattered electron zoning, and SHRIMP U-Pb geochronology of zircon and monazite, Geol Soc. Am. Bull., 118, 39-64, 2006.

Horn, I., and von Blanckenburg, F.: Investigation on elemental and isotopic fractionation during 196 nm femtosecond laser ablation multiple collector inductively coupled plasma mass spectrometry. Spectrochim. Acta. B, 62, 410-422, 2007.

Ludwig, K. R.: User's manual for Isoplot 3.75: A geochronological toolkit for Microsoft Excel, Berkeley Geochronology Center Special Publication, 5, 75, 2012.

McFarlane, C. R.: Allanite UPb geochronology by 193 nm LA ICP-MS using NIST610 glass for external calibration. Chem. Geol., 438, 91-102, 2016.

McFarlane, C. R., and Luo, Y.: U-Pb geochronology using 193 nm Excimer LA-ICP-MS optimized for in situ accessory mineral dating in thin sections. Geosci. Can., 39, 158-172, 2012.

Ntaflos, T., Bizimis, M., and Abart, R.: Mantle xenoliths from Szentbékálla, Balaton: Geochemical and petrological constraints on the evolution of the lithospheric mantle underneath Pannonian Basin, Hungary. Lithos, 276, 30-44, 2017.

Oberli, F., Meier, M., Berger, A., Rosenberg, C. L., and Gieré, R.: U-Th-Pb and 230Th/238U disequilibrium isotope systematics: Precise accessory mineral chronology and melt evolution tracing in the Alpine Bergell intrusion. Geochim. Cosmochim. Ac., 68, 2543-2560, 2004.

Paton, C., Hellstrom, J., Paul, B., Woodhead, J., and Hergt, J.: Iolite: Freeware for the visualisation and processing of mass spectrometric data. J. Anal. Atom. Spectrom., 26, 2508-2518, 2011.

Paton, C., Woodhead, J. D., Hellstrom, J. C., Hergt, J. M., Greig, A., and Maas, R.: Improved laser ablation U-Pb zircon geochronology through robust downhole fractionation correction. Geochem. Geophy. Geosy., 11, 2010.

Petrus, J. A., and Kamber, B. S.: VizualAge: A novel approach to laser ablation ICP-MS U-Pb geochronology data reduction, Geostand. Geoanal. Res., 36, 247-270, 2012.

Pouchou, J. L., and Pichoir, F.: Quantitative analysis of homogeneous or stratified microvolumes applying the model “PAP”, in: Electron Probe Quantitation, edited by Heinrich, K.F.J., Newbury, D.E., Springer, Boston, MA, 31-75, 1991.

Rudnick, R. L., and Gao, S.: Composition of the continental crust, in: Treatise on Geochemistry (Vol. 3), edited by Holland, H.D., Turekian, K.K., Elsevier–Pergamon, Oxford, 1–64, 2003.

Savitzky, A., and Golay, M. J.: Smoothing and differentiation of data by simplified least squares procedures, Anal. chem., 36, 1627-1639, 1964.

Vermeesch, P.: IsoplotR: A free and open toolbox for geochronology, Geosci. Front., 9, 1479-1493, 2018.